

Vectorial Doppler complex spectrum and its application to the rotational detection

Shuxian Quan, Ling Chen,* Siyao Wu, and Baocheng Zhang†

School of Mathematics and Physics, China University of Geosciences, Wuhan 430074, China

Vectorial polarized fields of light has been applied to detect the rotational velocity by the rotational Doppler effect, but the measurement was made for the rotation of a single-particle system. When the rotational surface is rough, the scattered vectorial Doppler signal spectrum is complex. In this paper, we make the complex spectrum analyses using orbital angular momentum modal expansion method. It is found that the highest peak in the Fourier form of the complex spectrum is obtained at the frequency shift $2l\Omega$ related to the topological charge (l) of the incident vortex light and the rotational velocity (Ω) of the rough surface. Based on the complex spectrum analysis, we construct a method to measure the magnitude and direction of the rotational velocity simultaneously for a general object, which has the practical application in remote sensing and astronomy.

I. INTRODUCTION

The concept of optical vortices was put forward firstly in 1989 [1], and soon after that it was shown that the optical vortices formed by Laguerre-Gaussian (LG) beams had an orbital angular momentum (OAM) appearing in the phase as $\exp(il\phi)$, where l is the topological charge (TC) [2] and determines the OAM value ($l\hbar$) of the photon, and ϕ is the azimuthal angle around the rotating axis. Through about 30 years of development, the optical vortex has been applied to many different fields such as optical communication, quantum information and so on [3].

Theoretically, it was suggested in 1996 that the optical vortex could be applied to measure the rotation rate of a spinning object [4]. When the vortex beam is scattered by the rotating object, the frequency shift in the OAM of the light is observed to deduce the rotation rate. The frequency shift, in essence, is stemmed from the Doppler effect [5], and this phenomenon is also called the rotational Doppler effect (RDE) [6–11]. In 2013, the RDE was first used for the detection of a spinning object in the experiment [12, 13], where it was confirmed that the RDE works even for the case that the angular momentum vector of the rotating object is parallel to the observation direction. Since then, the RDE is also applied to detect the rotation for the different macro and micro targets (see the review [14] and references therein). When the spinning object has a rough surface, the RDE can still be used to measure the object's rotation rate. But the spectrum for the scattered light by the rough surface is complex, the analyses for the spectrum is significant for the measurement and it is usually made using a method of the expansion of the different OAM components corresponding to different values of TC [15–19].

All those above are based on scalar vortex beams in which the spatial polarization has a fixed distribution, so the magnitude of the rotating velocity can be, but the

direction of the rotation cannot be determined in those cases. A recent attractive study [20, 21] using the cylindrical vectorial polarization fields (CVPFs) [22–25] presented the simultaneous measurement for the magnitude and direction of the velocity of a rotating particle. The so-called CVPFs are characterized by spatially and cyclically variant polarized fields across the transverse plane of the beams and polarization vortices could be formed. In this recent study, the beam with the CVPFs was illuminated on the rotating particle, and the relative phase difference between the two beams was observed to determine the velocity vector (magnitude and direction). However, they present only the measurement for the rotation of a single particle mimicked by a digital micromirror device (DMD) (see also other related measurements in Ref. [26, 27]), which is equivalent to the result from the rotation of uniformly isotropic and homogeneous surface. Whether it can be applied to measure the rotation of a rough surface is unclear directly since the inhomogeneous property of the rough surface could lead to complex Doppler speckle signals after the beams were illuminated on the rotating rough surface.

In this paper, we study the measurement of the velocity vector in a transverse plane normal to the light axis for a rotating tinfoil whose surface is rough using the CVPFs. We make the theoretical analyses for the complex spectrum scattered by the rotating rough surface, which has not been studied for the CVPFs before. We also measure the Doppler frequency shift using a paraxial two-path polarization detection method, in which the noises stemming from the low frequency terms in the complex spectrum can be suppressed. Our results show that the simultaneous measurement for the magnitude and direction of the velocity in a transverse plane normal to the light axis is still feasible. The extension of the vectorial Doppler metrology method to the general rotating objects is significant in the actual detection and has the potential to apply in remote sensing and astronomy.

*Electronic address: lingchen@cug.edu.cn

†Electronic address: zhangbaocheng@cug.edu.cn

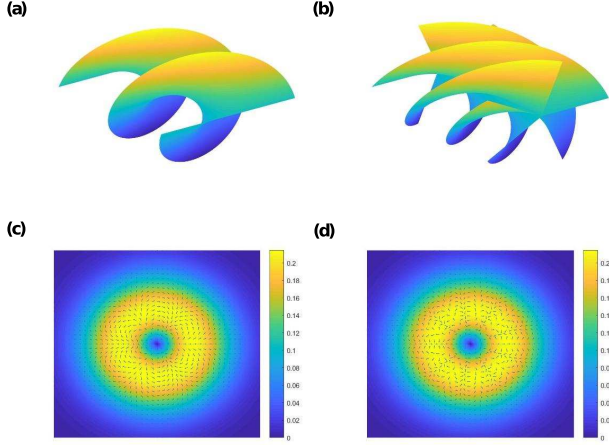


FIG. 1: Schematic diagram of optical vortices. The phase wavefront of scalar vortex beams are presented in (a) for the TC $l = 2$ and in (b) for the TC $l = 5$. The polarization distribution of vectorial vortex beams in the transverse plane are presented in (c) for TC $l = 2$ and in (d) for the TC $l = 5$.

II. SCATTERED LIGHT

We start with the consideration of a general CVVPF, whose light field is expressed using the Jones matrix as

$$\vec{E} = \vec{E}_0(r, z) e^{-2\pi i f t} \begin{pmatrix} \cos(l\phi + \alpha) \\ -\sin(l\phi + \alpha) \end{pmatrix}, \quad (1)$$

which can be generated by the superposition of one right-hand polarized vortex beam with TC l and one left-hand polarized vortex beam with TC $(-l)$. The two beams have the same field amplitude $\vec{E}_0(r, z)$ at the overlapped position (r, z) and have the same frequency f . For the CVVPFs, l is also understood as the order number of the polarization which represents the rotating cycles of the polarization vector, ϕ is the azimuthal angle, and α is the initial phase. It is easy to see that the polarization of the CVVPFs is dependent on spatial positions, as presented in Fig. 1. Compare it with the field of scalar vortex light which is expressed as $E_l = E_0(r, z) e^{il\theta} e^{-2\pi i f t}$. In the transverse direction perpendicular to the propagation direction of the vortex beam, the field E_l or its polarization is evenly distributed, as presented in Fig. 1.

When the vectorial beam is illuminated on a rough surface, its phase will be modulated according to the modulation function [28] as $M(r, \phi, t) = e^{i\varphi(r, \phi)} = \sum_k A_k(r) e^{ik\phi}$ where $A_k(r)$ is a complex amplitude of k -order modulation factor and satisfies the normalization $\sum_k |A_k(r)|^2 = 1$. If the rough surface is rotated with the angular frequency Ω , the modulation function becomes $M(r, \Omega, t) = e^{i\varphi(r, \theta - \Omega t)} = \sum_k A_k(r) e^{ik\phi} e^{-ik\Omega t}$.

After the vortex beam is scattered by the rough surface of the rotating body, the light field becomes

$$\vec{E}_s = M(r, \Omega, t) \vec{E}, \quad (2)$$

where $\vec{E}_0(r, z) e^{-2\pi i f t}$ is ignored for simplicity because only the change along the angular direction of the scattered light field is required in the paper. It is calculated further as

$$\vec{E}_s = \vec{E}(r) \begin{pmatrix} G \cos(\alpha + l\Omega t) + iF \sin(\alpha + l\Omega t) \\ -G \sin(\alpha + l\Omega t) + iF \cos(\alpha + l\Omega t) \end{pmatrix}, \quad (3)$$

which can be divided into the superposition of two beams with different polarizations,

$$\vec{E}_s = G \begin{pmatrix} \cos(\alpha + l\Omega t) \\ -\sin(\alpha + l\Omega t) \end{pmatrix} + iF \begin{pmatrix} \sin(\alpha + l\Omega t) \\ \cos(\alpha + l\Omega t) \end{pmatrix}, \quad (4)$$

where Ω is the angular frequency of the rotating body. The modulation functions

$$G = \sum_{m=-N}^N (A_{m-l} + A_{m+l}) e^{-im\Omega t} e^{im\phi}, \quad F = \sum_{m=-N}^N (A_{m-l} - A_{m+l}) e^{-im\Omega t} e^{im\phi}$$

where m represents the OAM mode of the scattered light, and $m = k + l$. G can be regarded as the superposition of different harmonic oscillations with the frequency $m\Omega$ and amplitude $A_{m-l} + A_{m+l}$, and F can be regarded as the superposition of different harmonic oscillations with the frequency $m\Omega$ and amplitude $A_{m-l} - A_{m+l}$ but along the direction perpendicular to that for G . According to Eq. (4), the scattered field can be obtained by a rotation at the angle $l\Omega t$ (in our paper the counterclockwise direction is defined as positive) for the CVVPFs with the form $(G, F)^T$ whose polarization distribution is not fixed and changes with time. In particular, if the angular frequency Ω remains unchanged but the direction of rotation is reversed (i.e. Ω becomes $-\Omega$ in Eq. (4)), the scattered field will be changed, i.e. $\vec{E}_s(-\Omega, t) \neq \vec{E}_s(\Omega, t)$, which shows that the polarization distribution in the scattered CVVPFs depends on the direction of the rotation. This provides a method to detect the direction of a rotation.

When the scattered light goes through a polarizer with the angular θ relative to the horizontal direction, the light field becomes

$$\begin{aligned} \vec{E}_{sf} &= \begin{bmatrix} \cos\theta & \sin\theta \\ 0 & 0 \end{bmatrix} \vec{E}_s \\ &= G \begin{bmatrix} \cos(l\Omega t + \theta) \\ 0 \end{bmatrix} + iF \begin{bmatrix} \sin(l\Omega t + \theta) \\ 0 \end{bmatrix}, \end{aligned} \quad (5)$$

where the initial phase $\alpha = 0$ is taken for simplicity. The light intensity is obtained as

$$\begin{aligned} I_j &= |G|^2 \cos^2(l\Omega t + \theta) + |F|^2 \sin^2(l\Omega t + \theta) \\ &+ \frac{1}{2} i(G^* F - GF^*) \sin 2(l\Omega t + \theta), \\ &= \frac{1}{2} (|G|^2 - |F|^2) \cos 2(l\Omega t + \theta) \\ &+ \frac{|G|^2 + |F|^2}{2} + \frac{1}{2} i(G^* F - GF^*) \sin 2(l\Omega t + \theta), \end{aligned} \quad (6)$$

where $*$ represents the complex conjugation, and the relations $\cos^2(l\Omega t + \theta) = \frac{1 + \cos 2(l\Omega t + \theta)}{2}$ and $\sin^2(l\Omega t + \theta) = \frac{1 - \cos 2(l\Omega t + \theta)}{2}$ are used. Although the last term has the imaginary number i in the result, but the term $i(G^*F - GF^*)$ is real, as calculated below.

To simplify the expression of the intensity, we have to calculate the terms related to modulation functions. At first, we calculate the term $|G|^2$ as

$$\begin{aligned} |G|^2 &= GG^* \\ &= \sum_{m,m'} (A_{m-l} + A_{m+l}) (A_{m'-l}^* + A_{m'+l}^*) e^{i(m-m')(\phi + \Omega t)} \end{aligned} \quad (7)$$

It can be seen that the right term is real by taking $m - m' = n$ where n is an integer in the range from 0 to $2m$. When $m - m' = n$, $|G|^2 = \sum_m (A_{m-l} + A_{m+l}) (A_{m+n-l}^* + A_{m+n+l}^*) e^{in(\phi + \Omega t)}$; when $m - m' = -n$, $|G|^2 = \sum_m (A_{m+n-l} + A_{m+n+l}) (A_{m-l}^* + A_{m+l}^*) e^{-in(\phi + \Omega t)}$. These two terms are complex conjugated, so their sum is real. Since the n term and the $(-n)$ term appear with pairs and they are complex conjugated, the total sum are real.

Similarly, we can calculate the term $|F|^2$ as

$$\begin{aligned} |F|^2 &= FF^* \\ &= \sum_{m,m'} (A_{m-l} - A_{m+l}) (A_{m'-l}^* - A_{m'+l}^*) e^{i(m-m')(\phi + \Omega t)}. \end{aligned} \quad (8)$$

It is also real. Then, we calculate

$$\begin{aligned} &\frac{1}{2} (|G|^2 - |F|^2) \\ &= \sum_{m,m'} (A_{m-l}A_{m'+l}^* + A_{m+l}A_{m'-l}^*) e^{i(m-m')(\phi + \Omega t)}, \\ &= \sum_{m,n} [(A_{m-l}A_{m+n+l}^* + A_{m+l}A_{m+n-l}^*) e^{in(\phi + \Omega t)} + c.c.], \end{aligned} \quad (9)$$

where $c.c.$ represents the complex conjugation of the former terms. Now we write these expressions in the actual form. At first, we analyze such sum: $(a + bi)e^{i\phi} + (a - bi)e^{-i\phi} = 2a \cos \phi - 2b \sin \phi = 2\sqrt{a^2 + b^2} (\frac{a}{\sqrt{a^2 + b^2}} \cos \phi - \frac{b}{\sqrt{a^2 + b^2}} \sin \phi) = 2\sqrt{a^2 + b^2} (\cos \phi' \cos \phi - \sin \phi' \sin \phi) = 2\sqrt{a^2 + b^2} \cos(\phi' + \phi)$ where $\sqrt{a^2 + b^2}$ and ϕ' are the modulus and argument of the complex number $(a + bi)$. Since the summation terms in Eqs. (7) and (8) are complex conjugated pairwise, thus according to the analysis above we obtain

$$\begin{aligned} &\frac{1}{2} (|G|^2 - |F|^2) \\ &= 2 \sum_{m,n} (|A_{m-l}| |A_{m+n+l}^*| \cos(n(\phi + \Omega t) + \varphi_n^{-l}) \\ &\quad + |A_{m+l}| |A_{m+n-l}^*| \cos(n(\phi + \Omega t) + \varphi_n^l)), \end{aligned} \quad (10)$$

where φ_n^{-l} and φ_n^l are the arguments of the complex numbers $A_{m-l}A_{m+n+l}^*$ and $A_{m+l}A_{m+n-l}^*$. Using the same analyses, we obtain

$$\begin{aligned} &\frac{1}{2} (|G|^2 + |F|^2) \\ &= 2 \sum_{m,n} (|A_{m-l}| |A_{m+n-l}^*| \cos(n(\phi + \Omega t) + \psi_n^{-l}) \\ &\quad + |A_{m+l}| |A_{m+n+l}^*| \cos(n(\phi + \Omega t) + \psi_n^l)), \end{aligned} \quad (11)$$

where ψ_n^{-l} and ψ_n^l are the arguments of the complex numbers $A_{k-l}A_{k+p+l}^*$ and $A_{k+l}A_{k+p-l}^*$, and

$$\begin{aligned} &\frac{1}{2} i(G^*F - GF^*) \\ &= -2 \sum_{m,n} (|A_{m-l}| |A_{m+n+l}^*| \sin(n(\phi + \Omega t) + \varphi_n^{-l}) \\ &\quad + |A_{m+l}| |A_{m+n-l}^*| \sin(n(\phi + \Omega t) + \varphi_n^l)). \end{aligned} \quad (12)$$

Then substitute Eqs. (10)-(12) into the expression (6) of light intensity, and we obtain

$$\begin{aligned} I &= \left| \vec{E}_{sf} \right|^2 = 2 \sum_{n=0}^N \sum_{m=-Z}^{Z-n} [|A_{m+l}| |A_{m+n-l}^*| \\ &\quad \times \cos((2l+n)\Omega t + n\phi + 2\theta + \varphi_n^l) \\ &\quad + |A_{m-l}| |A_{m+n+l}^*| \cos((2l-n)\Omega t - n\phi + 2\theta - \varphi_n^{-l}) \\ &\quad + |A_{m+l}| |A_{m+n+l}^*| \cos(n\Omega t + n\phi + \psi_n^l) \\ &\quad + |A_{m-l}| |A_{m+n-l}^*| \cos(n\Omega t + n\phi + \psi_n^{-l})]. \end{aligned} \quad (13)$$

When $n = 0$, the last two term becomes $\sum_m |A_{m+l}|^2 + \sum_m |A_{m-l}|^2$ which are independent on the rotational angular frequency. n , N , and Z are positive integers. Z is the detectable maximal TC, and the detectable TCs are $0, \pm 1, \pm 2, \dots, \pm Z$ for the symmetrical measurement. $N = 2Z$ represents the modes of beat frequency, which means the maximal difference between two arbitrary modes from $-Z$ to Z . For a given n -order harmonic component, there exist $(N - n + 1)$ terms contributed to the intensity. An illuminated interpretation is presented in Fig. 2.

The intensity I consists of four terms, but only the former two terms are related to the angle of polarizer. This provides the possibility to detect the rotation velocity by changing the angle of the polarizer. We called them beat frequency terms, which include different beat frequencies with the central frequency $2l\Omega/2\pi$, i.e. $2l\Omega/2\pi$, $(2l \pm 1)\Omega/2\pi$, $(2l \pm 2)\Omega/2\pi$, $(2l \pm 3)\Omega/2\pi$, \dots . The other two terms are called as low frequency terms. Theoretically, the scattered light should contain all possible modes, but in the practical experiment, only a small quantity of modes (i.e. N is small) can be measured. In particular, the amplitude of the mode with frequency $2l\Omega/2\pi$ is maximal, as seen in Fig. 2.

From the calculation above, it is seen that the distribution for the amplitude and direction of the polarization

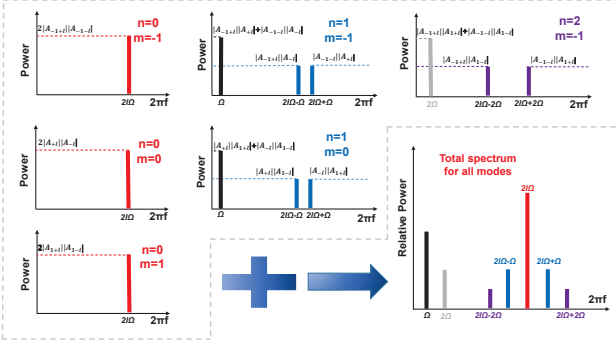


FIG. 2: Schematic diagram of complex spectrum with $Z = 1, N = 2$ in Eq. (13). The figures in the same row are presented with the same scattering mode m but different harmonic order n , and the figures in the same column are presented with the same harmonic order n but different scattering mode m . Here we assume that the modulated amplitudes of scattered light by the rough surface are the same. The figure in the lower right corner represents the complex spectrum by summing all these components, which gives the maximal amplitude at the frequency $2l\Omega$.

depends on the angle position ϕ in the transverse plane perpendicular to the propagation direction of the light. Meanwhile, in the process of light propagation, the distribution is rotated with a frequency $l\Omega$, and the rotation chirality for the polarization distribution will be changed if the direction of the rotating rough surface is changed. These provide the basis for detecting the amplitude and direction of the rotating objects.

A particular operation has to be stressed here. As calculated in Eq. (5), a polarizer is added before the detection for the scattered light. If the polarizer is not added, the detected light intensity is $I = E^*E = G^2 + F^2$ which includes only some low frequency terms unrelated to the TC of the incident light, similar to the last two terms in Eq. (13). This cannot provide the method to detect the direction of the rotation. When the polarizer is added, the beat frequency terms appear in the final expression for the light intensity as given in the former two terms in Eq. (13), which makes the detection of the direction possible. This is different from the scalar light field. If the incident light is scalar, the scattered light is also scalar. Thus, even if the polarizer is added before the detection, only the amplitude of the scalar light is modulated (i.e. $I \propto f(\theta) \cos(2l\Omega t + \alpha)$, θ is the angle of the added polarizer and $f(\theta)$ is a function related to the modulated amplitude) and so the direction cannot be detected in this case.

Then, a question is how to find the correspondence between the peak of the light intensity curve and the frequency since the scattered light field is so complex. At first, we explain the relationship between the parameters A, m and the rough degree of the rough surface. m is determined by the height from the reference plane to the surface of the material, and A is determined by the

surface area of the material at the same height. In our experiment, the fluctuation of the height in the surface of the tinfoil is at the micron scale, which lead to the small change for A and m in the different positions. So in the expansion of Eq. (13), the parameters $|A_m|$ have the approximately same value. Thus, we can estimate which frequency corresponds to the highest peak in the Fourier form of the spectrum by a simple calculation using Eq. (13). In our experiment, we use the paraxial symmetric measurement, in which the symmetric modes such as $0, \pm 1, \pm 2$ and so on are collected into the detector. Generally, when the maximal detectable mode is m , there are $2m$ terms for the low frequency modes, and there are $4m + 1$ terms for the beat frequency modes with the central frequency $2l\Omega$. Note that the contribution for the mode of frequency $2l\Omega$ is from $2m + 1$ terms and every term contributes to the amplitude by $2A^2$, and thus, the total contribution is $(4m + 2)A^2$, which leads to the highest peak in the spectrum curve. An illuminated interpretation is presented in Fig. 2 with the maximal detectable mode is 1. In this figure, every row represents the beat frequencies between the same mode with all possible modes, i.e. the first row presents the beat frequencies between the mode with $m = -1$ and the modes with $m = -1, 0, 1$ which corresponds to the harmonic orders $n = 0, 1, 2$; the second row presents the beat frequencies between the mode with $m = 0$ and the modes with $m = 0, 1$ which corresponds to the harmonic orders $n = 0, 1$; the third row presents the beat frequencies between the mode with $m = 1$ and the mode with $m = 1$ which corresponds to the harmonic order $n = 0$. According to Eq. (13), the harmonic order $n = 0$ corresponds to the peak at the frequency $2l\Omega$, and there are three terms contributed to the intensity with every one $2A^2$. The intensity at other frequency can be counted with such a method, as presented in the final plot (Total spectrum for all modes) in Fig. 2.

To confirm our theoretical analyses, Fig. 3a presents the Fourier transformed form of the complex spectrum measured in the experiments, in which the signals from the low frequency terms and the beat frequency terms in Eq. (13) can be found obviously. It is seen that the highest peak appears at the low frequency Ω , different from our theoretical estimation (the highest peak should be at the frequency $2l\Omega/2\pi$, as analyzed in SM). This could be caused by the noises from the mechanical vibration of the rotation motor. In order to improve the measurement results, either the noises should be subtracted using some specific methods, or the low frequency terms are subtracted in the final measured results. Whichever one is realized, the direct measurement for the light intensity is not feasible and some other operations are required. In the next section, we will discuss the measurement method and present the measurement process.

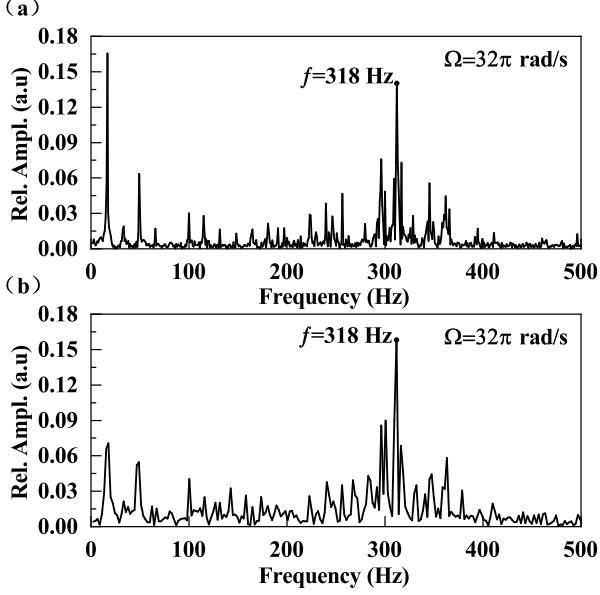


FIG. 3: Fourier transformation forms for measurement results of the complex spectrum with the angular velocity of rotation, $\Omega = 32\pi$ rad/s and the TC, $l = 10$, set in advance in our experiment. The down (up) plot indicates the results in which the low frequency terms are (are not) subtracted. The subtraction is made using the measurement results in the main path to subtract the results in the reference path, and then the Fourier transformation is made.

III. EXPERIMENTAL SETUP

As analyzed above for the complex spectrum of the scattered light, we can realize this by changing the angle θ of the polarizer. However, it is noted that the modes in the low frequency terms are independent of the angle θ , so it has to be subtracted in the measurement. For this, we use a beam splitter (BS) to divide the scattered light into two paths with the same amplitude in each path, as presented in Fig. 4 (the complete experimental setup is presented in Fig. 5, which contains three parts: the generation of CVPFs, the scattering of CVPFs by the rotating rough surface, and the detection of the scattering light). The path including a polarizer (P1) is regarded as the reference path and the angle of P1 is set at zero degree for the whole experiments. The path including the polarizer (P2) is called as the main path, and the measurement is realized by changing the angle of P2. For the measurement to obtain the magnitude of the rotational velocity, we can use the light intensity ($I_2(\theta)$) measured in the main path to subtract the light intensity

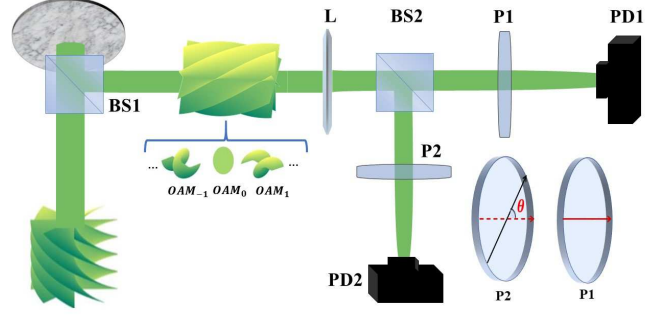


FIG. 4: Measurement method. The incident vectorial vortex light is scattered by the rotating rough surface. The scattered light is divided by the beam splitter (BS) into two paths. The path that the light goes through the polarizer (P1, its angle is set at the zero degree for the whole experiment) is the reference path. The path that the light goes through P2 (its angle will be changed according to the requirement of the measurement) is called as the main path.

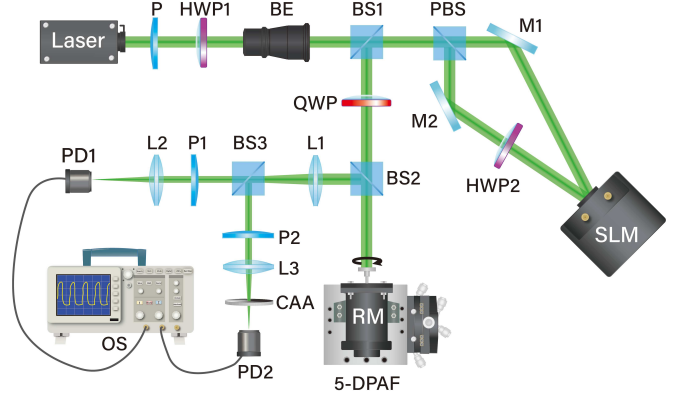


FIG. 5: Experimental setup. P, P1, P2: Polarizer; BE: Beam Expander; HWP1, HWP2: Half-Wave Plate; BS1, BS2, BS3: Beam Splitter; PBS: Polarization Beam Splitter; QWP: Quarter-Wave Plate; M1, M2: Mirror; SLM: Spatial Light Modulator; L1, L2, L3: Lens with the focal length 100 mm; PD1, PD2: Photodetector; OS: Oscilloscope; CAA: Continuously Adjustable Attenuator; 5-DPAF: Five Dimensional Precision Adjusting Frame; RM: Rotation Motor.

($I_1(\theta = 0)$) measured in the reference path,

$$\begin{aligned}
 I = I_2 - I_1 &= 4 \sin \theta \sum_{n=0}^N \sum_{m=-Z}^{Z-n} [|A_{m+l}| |A_{m+n-l}^*| \\
 &\times \sin((2l+n)\Omega t + n\phi + \theta + \varphi_n^l) \\
 &+ |A_{m-l}| |A_{m+n+l}^*| \sin((2l-n)\Omega t - n\phi + \theta_j - \varphi_n^{-l})], \quad (14)
 \end{aligned}$$

where Eq. (13) is used for the calculation. It is seen that the low frequency terms have been reduced. Then, we find the frequency relative to the maximal amplitude to deduce the value of the rotational velocity of the rough

surface using the relation $f = \frac{2l\Omega}{2\pi}$ for the known vortex beam with the TC l . For the measurement to obtain the direction of rotation, we can rotate the P2 in the main path along the same direction to increase the angle θ . The direction can be deduced by observing the shift of the spectrum line, and the detailed discussion is given below.

From Eq. (14), it is deduced that the highest peak in the frequency-domain spectrum curve corresponds to the beat frequency $2l\Omega/2\pi$, which is presented in Fig. 3b, as expected in the paraxial symmetrical measurement. It can be used to deduce the magnitude of rotational velocity. According to our measurement, the value of rotational velocity is 31.8π rad/s, which is nearly consistent with our setup (32π rad/s) for the rotation in advance. More similar cases are presented here, and all of them show that the subtraction is necessary to extract properly the frequency corresponding to the highest peak. Fig. 6 gives the results of the amplitude's change with the frequency under the conditions that the rotation velocity is the same, but the incident vectorial vortex beams are different with different TCs. Fig. 7 gives similar results but under different conditions that the incident vectorial vortex beams are the same and the rotation velocity is different. The left column in Fig. 6 and Fig. 7 presents the results measured in the main path, and the right column presents the difference of amplitude by subtracting the results measured in the reference path from the results measured in the main path. It is seen that the low-frequency terms are much suppressed in the right column of Fig. 6 and Fig. 7. At the same time, it is also seen that the highest peak is obtained at the frequency $2l\Omega$ in the right column of Fig. 6 and Fig. 7. Actually, the results are applicable in any other cases, but in our experiments, the rotation velocity cannot be set too large due to the limitation of the devices.

IV. MEASUREMENT RESULTS

Fig. 8 presents the measurement results for the magnitude of the rotational velocity. The data is obtained from the measurement of light intensity in the main optical path after subtracting the values from the reference path. The straight lines represent the theoretical results with the relation between the measured frequency at the maximal amplitude and the angular velocity of rotation, i.e. $f = 2l\Omega/2\pi$. It is seen that the measurement matches the theoretical results very well. Actually, this can also be used to measure the TC of the optical vortex given the rotational rate. Here we present the result of measuring the TC when the angular velocity of rotation is known, as in Fig. 9. In our measurement, if the rotation velocity is too small, the measurement will not be exact. This is because the measured results of light intensity in the two optical paths cannot be cancelled completely due to experimental errors. Thus, the low frequency terms will disturb the experimental results for the low rotation ve-

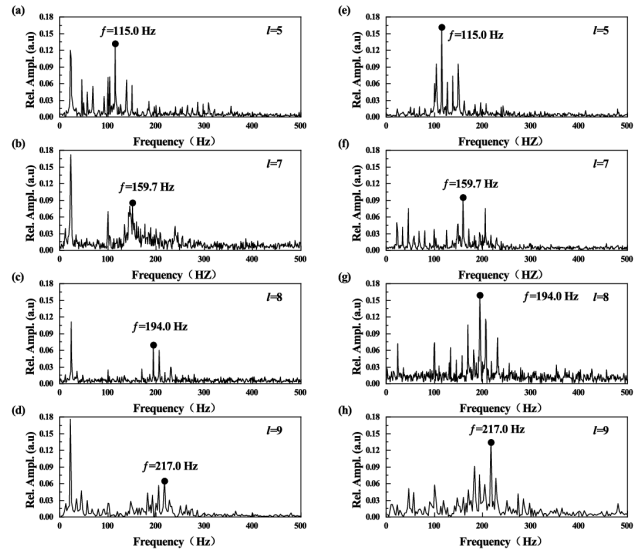


FIG. 6: Experimental results for the change of amplitude with the frequency under the same rotational velocity of the rough surface with $\Omega = 23\pi$ rad/s. The figures in (a-d) present the measured results in the main path and the figures in (e-f) present the difference between the measured results in the main path and those in the reference path.

locity.

Fig. 10 describes how to measure the direction of rotation. The method is to rotate the polarizer (P2) in the main optical path. From the left plot of Fig. 10, it is seen that the maximal amplitude for the beat frequency of the $2l\Omega/2\pi$ component will shift toward the leftside when the polarizer is rotated with the same direction with the detected rotation. Otherwise, when the polarizer is rotated with the inverse direction with the detected rotation, the measured maximal amplitude for the beat frequency of the $2l\Omega/2\pi$ component will shift toward the rightside. Thus, we can estimate the direction of rotation quickly and exactly by observing the shift of these curved lines. In particular, the results in Fig. 10 is obtained from the difference between the simultaneous measurements in the two paths. This can subtract the noises from the low frequency terms and from time difference for different angles of polarizer.

For the measurement of the rotational direction of the tinfoil, the subtraction of the results measured in the reference path is necessary. This, on one hand, can reduce the influence of the low frequency terms in the complex spectrum, and on the other hand, it can suppress the influence of the phase's errors due to the time difference for the measurements at different angles of polarizer, since the change of the angle requires to cost time, which leads to a new phase shift due to the time difference between two measurements at two different angles. Fig. 11 presents the results obtained only from the measurement in the main path without making the subtraction of the results measured in the reference path. It is seen that the

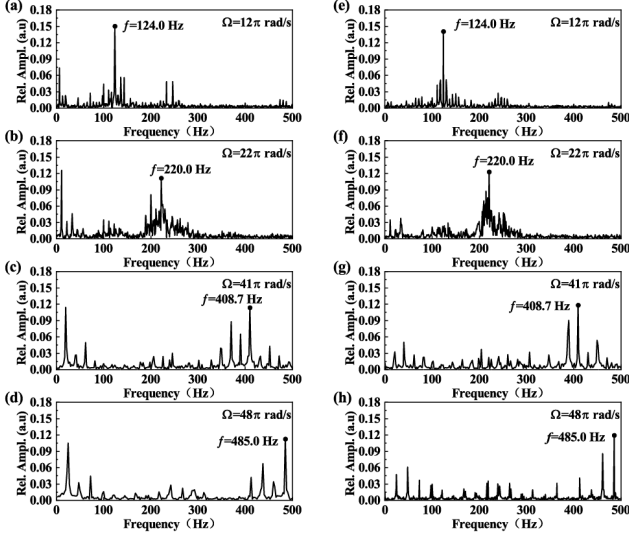


FIG. 7: Experimental results for the change of amplitude with the frequency under the same incident vortex beams with TC $l = 10$. The figures in (a-d) present the measured results in the main path and the figures in (e-f) present the difference between the measured results in the main path and those in the reference path.

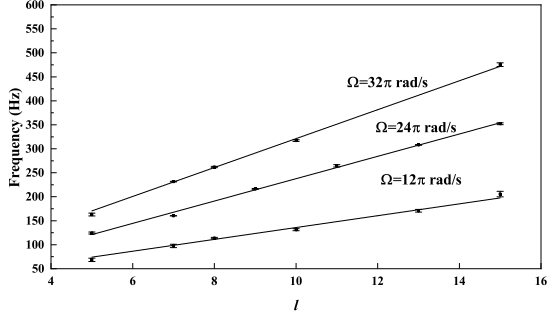


FIG. 8: Measurement results for the the angular velocity of rotation by the Doppler effect. The measurement results are obtained from the frequency at which the amplitude is maximal for every incident beam with TCs $l = 5, 7, 8, 9, 10, 11, 13, 15$. The error bars stems mainly from the mechanical vibration. The angular velocity of rotation is obtained by π times the slope of the lines.

shift could make mistakes for some changes in the angle of the polarizer. In fact, from Fig. 10, it is seen that only two lines for two different angles of the polarizer can lead us to deduce the rotational direction without any mistakes, but from Fig. 11, the errors occur, which might lead to the false estimation for the rotational direction due to the improper choices for the angles of the polarizer. However, the observation for the shift of the spectrum line from enough measurements at many different angles of the polarizer can also lead to the right estimation for the rotational direction.

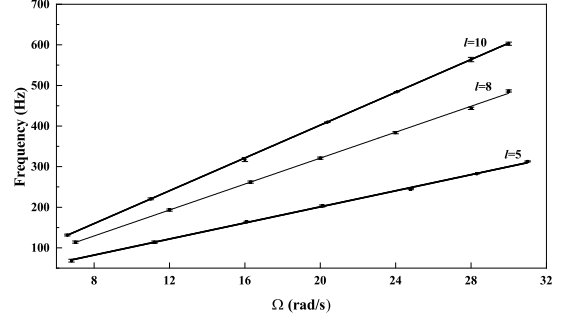


FIG. 9: Experimental results for the measurement of TC. The measurement results are obtained from the frequency at which the amplitude is maximum for different rotational velocity. The data points are obtained from the measurement results in the main path but subtracting the results in the reference path. They matches well with the theoretical results represented by the straight line. The TC can be deduced from the slope of the lines

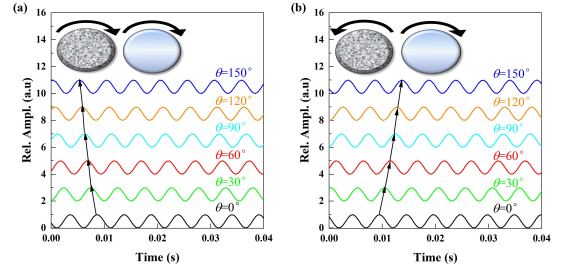


FIG. 10: Measurement results for the the direction of rotation. Signal modulation versus time are obtained by subtracting the results in the reference path from that in the main path and the different lines correspond to different angles of P2. The rough surface and the P2 are presented with the same rotation direction in (a) and the inverse direction in (b). The shift of spectra are marked with a line with the arrow.

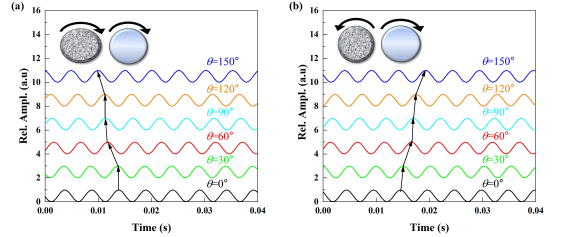


FIG. 11: Measurement results for the the direction of rotation. The change of amplitude with time are obtained from the measurement results in the main path and the different lines correspond to different angles of P2. The rough surface and the P2 are presented with the same rotation direction in (a) and the inverse direction in (b). The shift of spectra are marked with a line with the arrow.

V. CONCLUSIONS

In this paper, we investigate the rotational Doppler effect based on the CVPFs to detect the rotational velocity of a rough surface. We theoretically analyze the Doppler OAM complex spectrum which consists of the scattered light by a rough rotating surface, and obtain the expression for the intensity distribution of scattered light using the OAM modal expansion method. The highest peak in the Fourier form of the complex spectrum is found and it will be shifted if the polarizer is rotated, which provides the method to measure the magnitude and direction of the rotational velocity simultaneously. We also implement an experimental measurement for this based on a paraxial two-path method. One path is used as the reference to remove the noises related to the low frequency term in the complex spectrum and the time delay at the measurements for different angles of the polarizer in the main path. Different from the earlier measurement using the single-mode fiber to filter the specific mode, we use the paraxial symmetrical measurement to obtain the

complex spectrum within a small range of TC distribution. The highest peak and its shift following the rotation of the polarizer are measured. This gives the result about the rotational velocity, consistent with our theoretical analyses. Thus, we expand the method of vectorial Doppler metrology to the general situation, which goes forward a step to the practical application for the detection of rotation.

VI. ACKNOWLEDGMENTS

We acknowledge the support from the fund of China University of Geosciences (Wuhan). This work is also supported by the National Natural Science Foundation of China (NSFC) under Grant No. 11654001.

VII. REFERENCES

-
- [1] P. Couillet, L. Gil, and F. Rocca, Optical vortices. *Opt. Commun.* 73, 403 (1989).
- [2] L. Allen, M. W. Beijersbergen, R. J. C. Spreeuw, J. P. Woerdman, Orbital angular momentum of light and the transformation of Laguerre-Gaussian laser modes, *Phys. Rev. A* 45, 8185 (1992).
- [3] Y. Shen, X. Wang, Z. Xie, C. Min, X. Fu, Q. Liu, M. Gong, and X. Yuan, Optical vortices 30 years on: OAM manipulation from topological charge to multiple singularities. *Light: Science and Application* 8, 90 (2019).
- [4] G. Nienhuis, Doppler Effect induced by rotating lenses, *Optics Communications*, 132, 8 (1996).
- [5] Y. Yeh, H. Z. Cummins, Localized fluid flow measurements with an He-Ne laser spectrometer, *Appl. Phys. Lett.* 4, 176 (1964).
- [6] B. A. Garetz, Angular Doppler effect, *J. Opt. Soc. Am.* 71, 609 (1981).
- [7] I. Bialynicki-Birula, Z. Bialynicka-Birula, Rotational Frequency Shift, *Phys. Rev. Lett.* 78, 2539–2542 (1997).
- [8] J. Courtial, D. A. Robertson, K. Dholakia, L. Allen, and M. J. Padgett, Rotational frequency shift of a light beam, *Phys. Rev. Lett.* 81, 4828 (1998).
- [9] M. J. Padgett, Like a speeding watch, *Nature* 443, 924 (2006).
- [10] S. Barreiro, J. W. R. Tabosa, H. Failache, A. Lezama, Spectroscopic Observation of the Rotational Doppler Effect, *Phys. Rev. Lett.* 97, 113601 (2006).
- [11] A. Belmonte and J. P. Torres, Optical Doppler shift with structured light, *Opt. Lett.* 36, 4437 (2011).
- [12] L. Marrucci, Spinning the Doppler effect, *Science* 341, 464 (2013).
- [13] M. P. J. Lavery, F. C. Speirits, S. M. Barnett, and M. J. Padgett, Detection of a Spinning Object Using Light's Orbital Angular Momentum, *Science* 341, 537 (2013).
- [14] T. -Y. Cheng, W. -Y. Wang, J. -S. Li, J. -X. Guo, S. Liu, and J. -Q. Lü, Rotational Doppler Effect in Vortex Light and Its Applications for Detection of the Rotational Motion, *Photonics* 9, 441 (2022).
- [15] H. Zhou, D. Fu, J. Dong, P. Zhang, and X. Zhang, Theoretical analysis and experimental verification on optical rotational Doppler effect, *Opt. Express* 24, 010050 (2016).
- [16] H. Zhou, D. Fu, J. Dong, P. Zhang, D. Chen, X. Cai, F. Li, and X. Zhang, Orbital angular momentum complex spectrum analyzer for vortex light based on the rotational Doppler effect, *Light: Science & Applications* 6, e16251 (2017).
- [17] A. Q. Alexander, E. F. Strong, B. M. Heffernan, M. E. Siemens, G. B. Rieker, and J. T. Gopinath, Detection technique effect on rotational Doppler measurements, *Opt. Lett.* 45, 2636 (2020).
- [18] Y. Ding, Y. Ren, T. Liu, S. Qiu, Ch. Wang, Z. Li, and Z. Liu, Analysis of misaligned optical rotational Doppler effect by modal decomposition, *Opt. Express* 29, 15288 (2021).
- [19] S. Qiu, R. Tang, X. Zhu, T. Liu, and Y. Ren, Detection of a Spinning Object at Different Beam Sizes Based on the Optical Rotational Doppler Effect, *Photonics* 9, 517 (2022).
- [20] L. Fang, Z. Wan, A. Forbes, and J. Wang, Vectorial Doppler metrology, *Nat. Commun.* 12, 4186 (2021).
- [21] Z. Li, T. Liu, Y. Ren, S. Qiu, C. Wang, and H. Wang, Direction-sensitive detection of a spinning object using dual-frequency vortex light, *Opt. Express* 29, 7453 (2021).
- [22] Q. Zhan, Cylindrical vector beams: from mathematical concepts to applications. *Adv. Opt. Photon.* 1, 1 (2009).
- [23] H. M. Doleman, F. Monticone, W. den Hollander, A. Alù, and A. F. Koenderink, Experimental observation of a polarization vortex at an optical bound state in the continuum. *Nat. Photon.* 12, 397 (2018).
- [24] L. De Angells, T. Bauer, F. Alpeggiani, and L. Kuipers,

- Index-symmetry breaking of polarization vortices in 2D random vector waves. *Optica* 6, 1237 (2019).
- [25] C. He, J. Chang, Q. Hu, J. Wang, J. Antonello, H. He, S. Liu, J. Lin, B. Dai, D. S. Elson, P. Xi, H. Ma, and M. J. Booth, Complex vectorial optics through gradient index lens cascades, *Nat. Commun.* 10, 4264 (2019).
- [26] C. Rosales-Guzmán, N. Hermosa, A. Belmonte, and J. P. Torres, Direction-sensitive transverse velocity measurement by phase-modulated structured light beams, *Opt. Lett.* 39, 5415 (2014).
- [27] Z. Wan, L. Fang, and J. Wang, Direction-discriminated rotational Doppler velocimetry with circularly polarized vortex beams, *Opt. Lett.* 47, 1021 (2022) .
- [28] D. B. Phillips, M. P. Lee, F. C. Speirits, S. M. Barnett, S. H. Simpson, M. P. J. Lavery, M. J. Padgett, and G. M. Gibson, Rotational Doppler velocimetry to probe the angular velocity of spinning microparticles, *Phys. Rev. A* 90, 011801 (2014).